Electronic structure and orbital ordering of $SrRu_{1-x}Ti_xO_3$: GGA+U investigations

Pao-An Lin,[1] Horng-Tay Jeng,[1,2,*] and Chen-Shiung Hsue[2]
[1]*Institute of Physics, Academia Sinica, Taipei 11529, Taiwan*
[2]*Department of Physics, National Tsing Hua University, Hsinchu 30013, Taiwan*
(Received 6 September 2007; published 26 February 2008)

The electronic structures of the titanium-doped perovskite ruthenates $SrRu_{1-x}Ti_xO_3$ with $x=0.25$, 0.50, and 0.75 are investigated using the generalized gradient approximation (GGA) as well as the GGA plus Hubbard U (GGA+U) scheme. It is found that the Ti substitutions with nearly empty 3d orbitals and relatively smaller atomic sizes significantly affect the orbital ordering patterns on the Ru sublattices. In addition, the observed metal-insulator transition upon change in the Ti dopant concentration is demonstrated to be driven primarily by the on-site Coulomb correlation U. The good agreement between the GGA+U results and the experimental observations reveals that the electron correlation plays an important role in $SrRu_{1-x}Ti_xO_3$.

DOI: 10.1103/PhysRevB.77.085118 PACS number(s): 71.20.−b, 31.15.A−, 32.10.Dk

I. INTRODUCTION

Ruthenium-based oxides have attracted increasing attention in recent years because of their diverse electronic and magnetic properties as well as the unconventional superconductivity discovered in layered ruthenate Sr_2RuO_4.[1] With the substitution of Ca^{2+} for Sr^{2+} ions, Ca_2RuO_4 turns into an antiferromagnetic Mott insulator.[2] $SrRuO_3$ is known to be the only ferromagnetic metal ($T_c \approx 160$ K) among the 4d transition-metal oxides, whereas the magnetic properties of the metallic $CaRuO_3$ remain controversial. Although the electron correlation in the relatively itinerant Ru 4d orbitals is less important than that in 3d oxides, there have been many recent works focusing on the electron correlation effects in $SrRuO_3$ such as measurements on optical properties,[3] infrared and optical reflectivity,[4] thermal, magnetic, and transport properties,[5] and photoemission and x-ray absorption spectroscopy.[6–10]

The metal-insulator transition (MIT) in partially filled transition-metal oxides can be caused by either electron correlation[11] (Mott-Hubbard transition) or dopant-induced disorder[12] (Anderson transition) effects. With the correlated metallic Ru 4d band and nearly empty insulating Ti 3d bands properly separated, $SrRu_{1-x}Ti_xO_3$ serves as an ideal system for investigating the combined electron correlation and disorder effects on the MIT mechanism.[13–16] One of the end members, $SrRuO_3$ (Fig. 1), is a correlated ferromagnetic metal with partially filled 4d t_{2g} orbitals in Ru^{4+} ions. The other end member, $SrTiO_3$, is an optical band-gap insulator with a fully filled O 2p valence band and empty 3d orbitals for the Ti^{4+} ions. On mixing these two members, $SrRu_{1-x}Ti_xO_3$ goes from a correlated metal ($x=0.0$), to a disordered metal ($x \approx 0.3$), to an Anderson insulator ($x \approx 0.5$), to a soft Coulomb gap insulator ($x \approx 0.6$), to a disordered-correlation insulator ($x \approx 0.8$), to a band insulator ($x=1.0$),[15,16] with the MIT taking place at $x \approx 0.3$.[15,16] However, a larger x between 0.5 and 0.6 for the MIT was also reported in an earlier work.[13]

Orbital ordering, which is closely related to the charge, spin, and lattice degrees of freedom, is one of the most challenging topics in transition-metal oxides both experimentally[17,18] and theoretically.[19,20] In a previous paper,[20] we investigated the electronic structures of $SrRuO_3$ using the generalized gradient approximation plus Hubbard U (GGA+U) method. We found that the Ru spin-down electrons form a 4d t_{2g} orbital ordered ground state with canted d_{xz} and d_{yz} orbitals on the Ru1-Ru3 and Ru2-Ru4 sublattices, respectively. This finding unravels the close connection between the observed orbital ordering and the Jahn-Teller distortions, as well as the importance of the on-site correlation in the relatively extended Ru 4d orbitals.[20]

In this work, we present electronic structure calculations of $SrRu_{1-x}Ti_xO_3$. The computational details are described in the next section. The metal-insulator transition and the evolution of orbital ordering with increasing Ti dopant concentration are presented and discussed in Sec. III. The conclusions are given in Sec. IV.

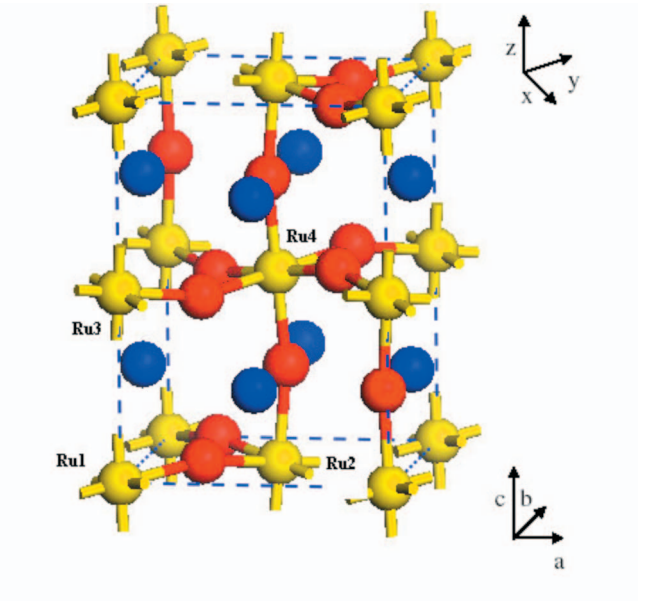

FIG. 1. (Color) Lattice structure of $SrRuO_3$. The yellow, red, and blue spheres denote the Ru, O, and Sr atoms, respectively. *abc* and *xyz* are respectively the crystal and local coordinates.

II. COMPUTATIONAL DETAILS

Band structure calculations for titanium-doped perovskite ruthenates $SrRu_{1-x}Ti_xO_3$ with x of 0.25, 0.50, and 0.75 were performed using the accurate full-potential projected augmented wave method[21] as implemented in the VASP package[22] within the generalized gradient approximation[23] as well as the GGA plus Hubbard U scheme.[24] The dopants in $SrRu_{1-x}Ti_xO_3$ were simulated by proper Ti substitutions for Ru ions in the supercell approach under structure optimizations based on the refined lattice structure of $SrRuO_3$.[25] For $x=0.25$ lattice, we replaced Ru1 (Fig. 1) by Ti (lattice I), while Ru1–Ru3 were substituted by Ti for $x=0.75$ (V). Three possible dopant configurations were calculated for $x=0.5$: the plane type in which Ru1 and Ru2 were replaced by Ti (II), the chain type in which Ru1 and Ru3 were replaced by Ti (III), and the diagonal type in which Ru1 and Ru4 were replaced by Ti (IV). The calculations were carried out over a $7\times7\times5$ Monkhorst-Pack k-point mesh in the irreducible Brillouin zone using 31 360 plane waves with cutoff energy of 400 eV. The on site Coulomb energy $U=3.5$ eV and exchange parameter $J=0.6$ eV (Ref. 26) were used for Ru ions to explore the correlation effects in the $4d$ orbitals, whereas we use $U=J=0.0$ eV for Ti ions due to the nearly empty valence $3d$ orbitals.

III. RESULTS AND DISCUSSION

A. Electronic structure

Figures 2(a)–2(e) demonstrate the total density of states (DOS) of $SrRu_{1-x}Ti_xO_3$ from GGA calculations for lattices I–V, respectively. The DOSs of the low-doping $x=0.25$ case [Fig. 2(a)] are basically similar to those of the undoped $SrRuO_3$.[20] The O $2p$ bands span from ~2 to ~8 eV below the Fermi level, while the main peaks of the spin-up and-down Ru t_{2g} bands are located at ~0.5 eV below and ~0.3 eV above the Fermi level, respectively, resulting in a metallic ferromagnetic ground state with the exchange splitting of ~0.8 eV. The Ru^{4+} ions are in the high-spin state with the spin alignment $(t_{2g}^3\uparrow, t_{2g}^1\downarrow)$, giving rise to a magnetic moment close to $2\mu_B$. Meanwhile, the crystal field splittings between the Ru t_{2g} and the higher Ru e_g bands are about 2 eV in both spin channels, whereas the nearly empty Ti $3d$ bands at ~2 eV above E_f are mixed with Ru e_g bands in energies.

For $x=0.5$, the DOSs of the plane [Fig. 2(b)] and chain [Fig. 2(c)] types are similar to the each other, and to some extent similar to the $x=0.25$ case. Since the two Ru ions in the diagonal-type lattice (IV) are relatively far away from each other, all the bandwidths are noticeably suppressed [Fig. 2(d)] due to the reduced overlaps among the electron clouds. Further, a crystal field energy gap at E_f in the spin-up channel is therefore opened up between the occupied Ru t_{2g} and unoccupied Ru e_g bands, giving rise to a half-metallic ground state with an integer magnetic moment of $1\mu_B$ per $SrRu_{0.5}Ti_{0.5}O_3$. The bandwidth suppression can be seen more clearly in the half-metallic $x=0.75$ case [Fig. 2(e)]. The Ru t_{2g} bandwidths are significantly reduced from ~2 eV for $x=0.25$ to less than 1 eV for $x=0.75$.

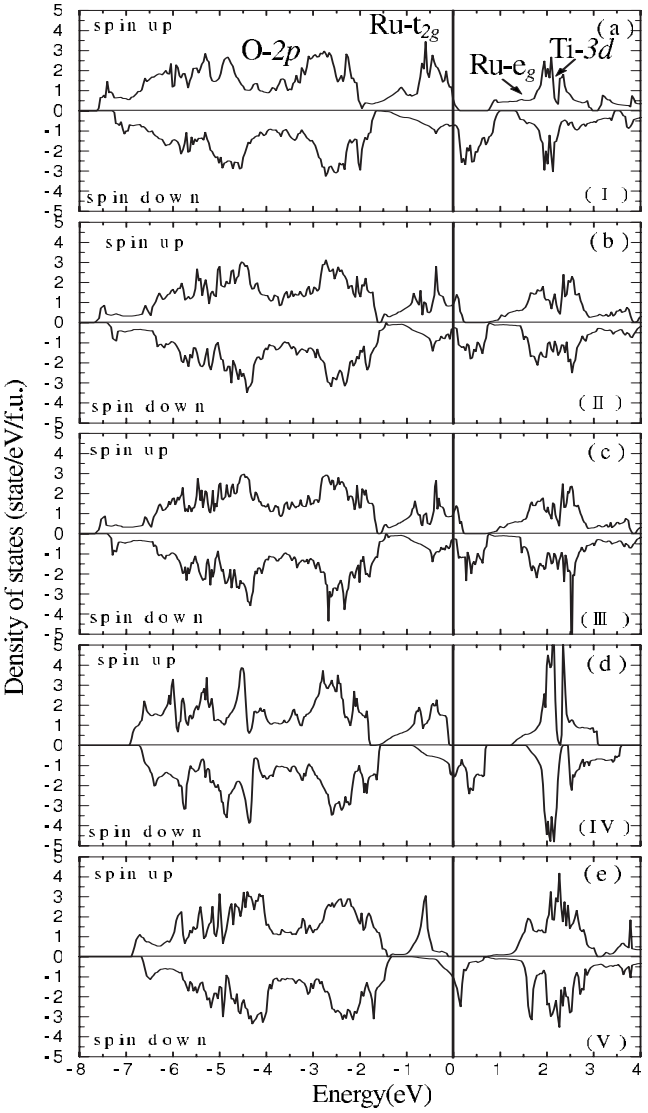

FIG. 2. Total DOS of $SrRu_{1-x}Ti_xO_3$ from the GGA. x=(a) 0.25 (lattice I), (b)–(d) 0.5 with different doping types (lattices II–IV, respectively), and (e) 0.75 (lattice V).

Although there exists a metal to half-metal transition at $x\approx0.5$ in the above GGA calculations (Fig. 2), the experimentally observed MIT at[15,16] $x\approx0.3$ was not successfully reproduced. The discrepancy indicates that the electron correlation plays an important role in the MIT mechanism. Figures 3(a)–3(e) illustrate the total DOSs of $SrRu_{1-x}Ti_xO_3$ in lattices I–V, respectively, from GGA+U calculations with $U=3.5$ eV. When the on-site Coulomb energy U, which localizes the Ru $4d$ orbitals and suppresses the bandwidths, is taken into account, $SrRu_{1-x}Ti_xO_3$ starts with a half-metallic ground state for $x=0.25$ [Fig. 3(a)]. This is consistent with the half-metallic ground state for the undoped $SrRuO_3$ given from GGA+U calculations.[20] For the three $x=0.5$ cases [Figs. 3(b)–3(d)], the DOSs of the spin-down Ru t_{2g} bands at E_f are strongly cut down so that the plane-type lattice (II) is close to an insulator with very limited DOS at E_f, while the chain (III) and diagonal (IV) lattice types turn out to be insulators with energy gaps of 0.05 and 0.1 eV, respectively.

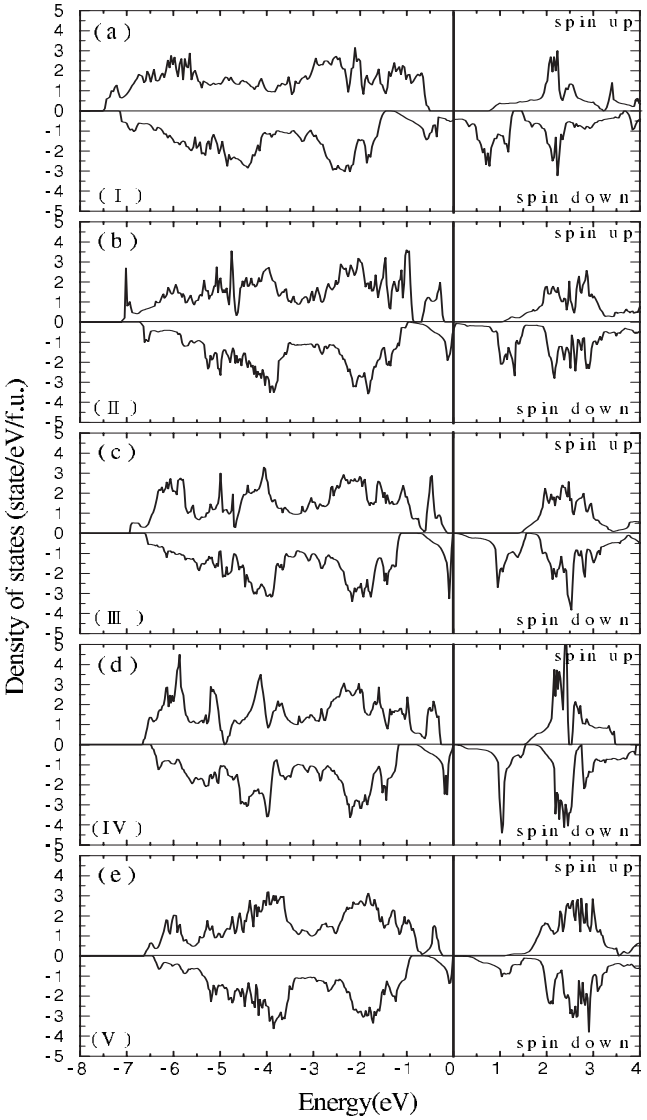

FIG. 3. Total DOS of $SrRu_{1-x}Ti_xO_3$ from GGA+U calculations. x=(a) 0.25 (lattice I), (b)–(d) 0.5 with different doping types (lattices II–IV, respectively), and (e) 0.75 (lattice V).

The GGA+U calculations successfully provide a MIT at $x \approx 0.5$, which is compatible with the experimental observation of the MIT at $x \approx 0.3$.[15,16]

The different electronic behavior of different doping types with $x=0.5$ can be related to the disorder effects.[12] In a randomly doped system, the conducting ions could be close to each other as in lattices II and III, away from each other as in lattice IV, or even far away from each other as in lattice V in different regions. Therefore the resistivity can be higher than it should be in a well-ordered case because of the distance fluctuations among the metallic ions, and of the strongly disordered potential[12] for the Bloch waves. In addition, it might also be related to a percolation transition, as for metals embedded in a rare gas matrix, responsible for the MIT.[27] As for $x=0.75$ case, the insulating spin-down energy gap of 0.2 eV at E_f is even clearer [Fig. 3(e)] since the first and second nearest neighbors are all Ti ions and electron hopping between conductive Ru ions is therefore unavailable in this case. The obtained energy gap of 0.2 eV is compatible with the optical gap of ~0.4 eV observed for the $x \sim 0.8$ case.[15,16]

To clarify the origin of the deviation between the MIT observed at $x \approx 0.3$[15,16] and the the MIT obtained at $x \approx 0.5$ (Fig. 3) using an electron correlation U of 3.5 eV. We present in Fig. 4 the DOS from GGA+U calculation using U of 3.0–4.5 eV. As can be seen clearly, a larger on-site Coulomb repulsion U of 4.0 and 4.5 eV would open up energy gaps of 0.02 and 0.24 eV, respectively, at E_f for lattice II, which would make the $x=0.5$ compound a Mott-Hubbard insulator. As a result, the MIT could take place at $x \approx 0.3$ if a larger Coulomb energy U is used in the GGA+U calculations. This is presumably because the Ru 4d orbitals in $SrRu_{1-x}Ti_xO_3$ are more localized due to the Ti^{4+} dopants with nearly empty valence orbitals than those in the undoped $SrRuO_3$. Therefore a larger U would be more reasonable for higher dopant concentrations. Combined with the GGA (Fig. 2) and GGA+U (Fig. 3) results, one may conclude that the MIT in $SrRu_{1-x}Ti_xO_3$ is driven mainly by the on-site Coulomb repulsion and partially by dose or disorder effects.

Previous photoemission and x-ray absorption[16] and optical and transport studies[15] on $SrRu_{1-x}Ti_xO_3$ demonstrated that the Ru t_{2g} bands play the main role in the MIT mechanism. In the following, we present the decomposed band structures near E_f for a close look at the Ru 4d band dispersions of different Ru concentrations. Figure 5 shows the site-decomposed band structure (BS) along the orthorhombic high-symmetry lines around E_f for $x=0.25$ case from GGA+U calculations. The sizes of the colored spheres represent the magnitudes of contributions from different Ru sites. It can be seen in the conducting minority spin channel that the Ru t_{2g} bands are relatively dispersive along GS, GX, and GY directions, indicating a better conductivity on lattice a-b plane. The band character is mainly Ru2 (red) at E_f, especially along GS and XY, which correspond to the lattice [110] and $[\bar{1}10]$ directions, respectively. Further along XY, the three occupied bands are well separated into Ru2 (red), Ru3 (green), and Ru4 (blue) bands. The Ru2 band has the highest energy close to E_f, while the Ru4 band is located at about ~−0.6 eV. The main part of the Ru3 band comes from the band maxima at X and Y points with energy of ~−0.4 eV. As will be discussed in Sec. III B, the three bands can be separated not only into Ru2, Ru3, and Ru4 sites but also into different cubic harmonic orbitals of different Ru sites.

Figure 6 depicts the site-orbital-decomposed minority BS around E_f for $SrRu_{0.5}Ti_{0.5}O_3$ in the plane-type lattice (II) from GGA+U calculations. The magnitudes of the contributions from different orbitals of Ru ions are indicated by the different sizes of the colored spheres. The highest occupied part (−1 to 0 eV) is composed mainly of two bands with the lower one belonging to Ru3 (left panel) and the higher one belonging to Ru4 (right panel). The lower Ru3 band is of mainly d_{xz} (purple) character, while d_{yz} (green) orbital predominates in the higher Ru4 band. This clearly indicates the formation of an orbital-ordered ground state as presented in Sec. III B. The site-orbital-decomposed BSs of the other two $x=0.5$ cases (lattices III and IV) are to some extent similar to that of lattice II with different orbital characters and gap openings due to the different doping types (not shown here).

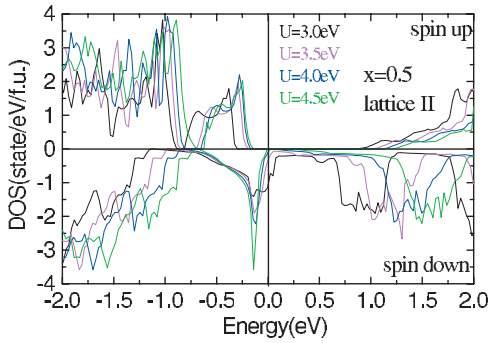

FIG. 4. (Color) Total DOS of $SrRu_{0.5}Ti_{0.5}O_3$ around E_f in plane-type lattice (II) from GGA+U calculations with U=3.0, 3.5, 4.0, and 4.5 eV.

The GGA+U site-decomposed BS of the x=0.75 case (lattice V) is presented in Fig. 7. There is one occupied Ru band for each spin channel with an indirect band gap of ~0.2 eV between G and X points in the minority spin channel. Orbital-decomposition analysis reveals that the occupied Ru band is still of 4d t_{2g} character because of the octahedral crystal field; however, the resultant electron cloud is a complicated linear combination of the three t_{2g} states in accordance with the lattice distortions as presented below.

B. Orbital ordering

By taking into consideration the on-site Coulomb correlation (GGA+U) in previous work,[20] we found for $SrRuO_3$ an orbital-ordered ground state, in which the four Ru ions can be divided into two groups according to the occupied orbital character, closely related to the associated Jahn-Teller distortion. The highest occupied bands in the minority spin channel of Ru1 and Ru3 are of predominantly d_{xz} and d_{xy} character, whereas those of Ru2 and Ru4 have mainly d_{yz} and d_{xy} features (Fig. 3 of Ref. 20). The 4d t_{2g} electron clouds on Ru1 and Ru3 ions arrange themselves in zigzag "ribbons" running parallel to the c axis, while those on the Ru2-Ru4 sublattice differ from the former by a 90° rotation about the c axis (Fig. 4 of Ref. 20).

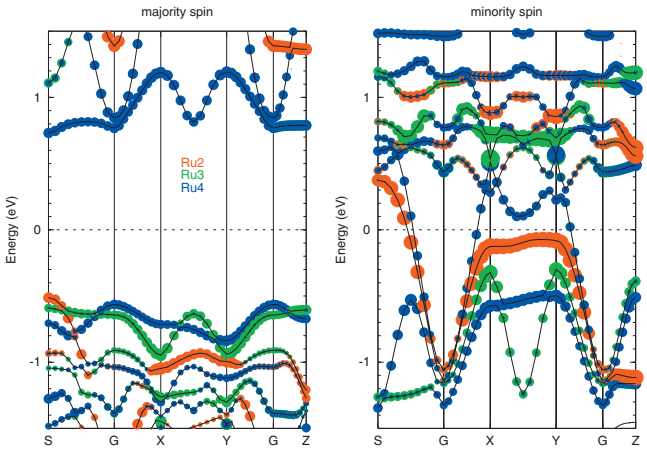

FIG. 5. (Color) Site-decomposed BS of $SrRu_{0.75}Ti_{0.25}O_3$ from GGA+U calculations with U=3.5 eV. The sizes of red, green, and blue spheres denote the contributions from Ru2, Ru3, and Ru4 ions, respectively.

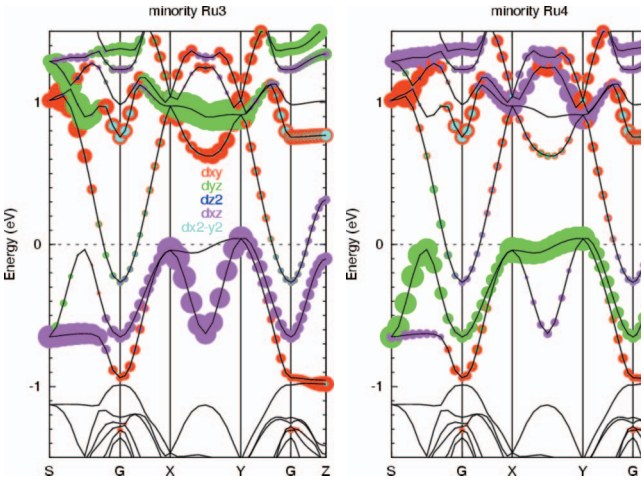

FIG. 6. (Color) Site-orbital-decomposed minority spin BS of $SrRu_{0.5}Ti_{0.5}O_3$ for Ru3 (left panel) and Ru4 (right panel) in plane-type lattice (II) from GGA+U calculations. The sizes of red, green, blue, purple, and light blue spheres denote the contributions from d_{xy}, d_{yz}, d_{z^2}, d_{xz}, and $d_{x^2-y^2}$ orbitals, respectively.

Figure 8(a) illustrates the GGA+U partial DOSs of the three Ru ions in $SrRu_{0.75}Ti_{0.25}O_3$ projected onto the five fold 4d orbitals in the local coordinates (xyz) with the z axis directed along the crystal c axis and the x and y axes pointing, respectively, to the crystal $[1\bar{1}0]$ and [110] directions. As can be seen, the highest occupied spin-down Ru band character is significantly different from that in the undoped $SrRuO_3$.[20] For Ru2 (top panel), this band belongs to the d_{xy} orbital instead of mixed $d_{yz}+d_{xy}$ orbitals as in $SrRuO_3$ since the d_{yz} band energy has been raised to ~0.7 eV above E_f. Meanwhile, the spin-down t_{2g} bands of Ru3 (middle panel) and Ru4 (bottom panel) are occupied by mainly d_{xz} and d_{yz} electrons, respectively. The occupied d_{xy} bands of both Ru3 and Ru4 in $SrRuO_3$ have been moved to 0.3–1.3 eV above E_f in $SrRu_{0.75}Ti_{0.25}O_3$. This is because the 3d Ti^{4+} ions are almost valence-electron-free, and the ion sizes are much

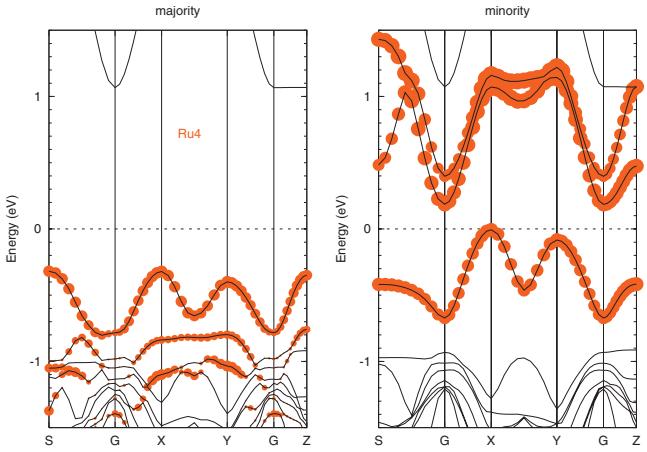

FIG. 7. (Color) Site-decomposed BS of $SrRu_{0.25}Ti_{0.75}O_3$ (lattice V) from GGA+U calculations. The size of the red spheres denote the contributions from Ru4 ions.

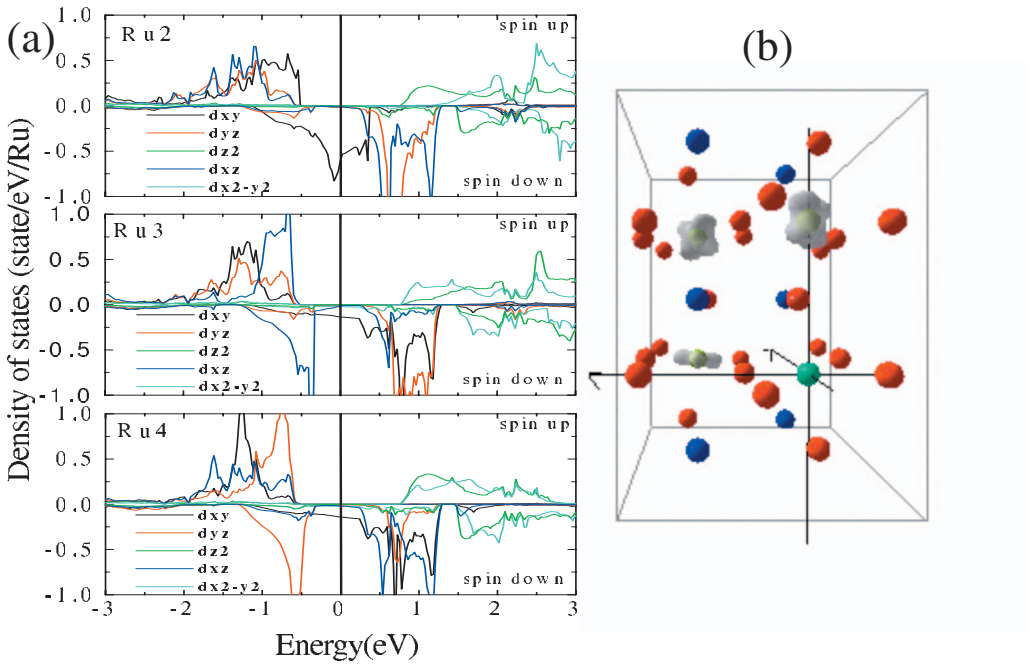

FIG. 8. (Color) Partial DOS (a) of Ru2 (top panel), Ru3 (middle panel), and Ru4 (bottom panel), and orbital ordering pattern (b) in $SrRu_{0.75}Ti_{0.25}O_3$ (lattice I) from GGA+U calculations. The blue, green, light blue, and red balls denote Sr, Ru, Ti, and O ions, respectively. The gray color illustrates the charge contour of the occupied spin-down Ru-t_{2g} band.

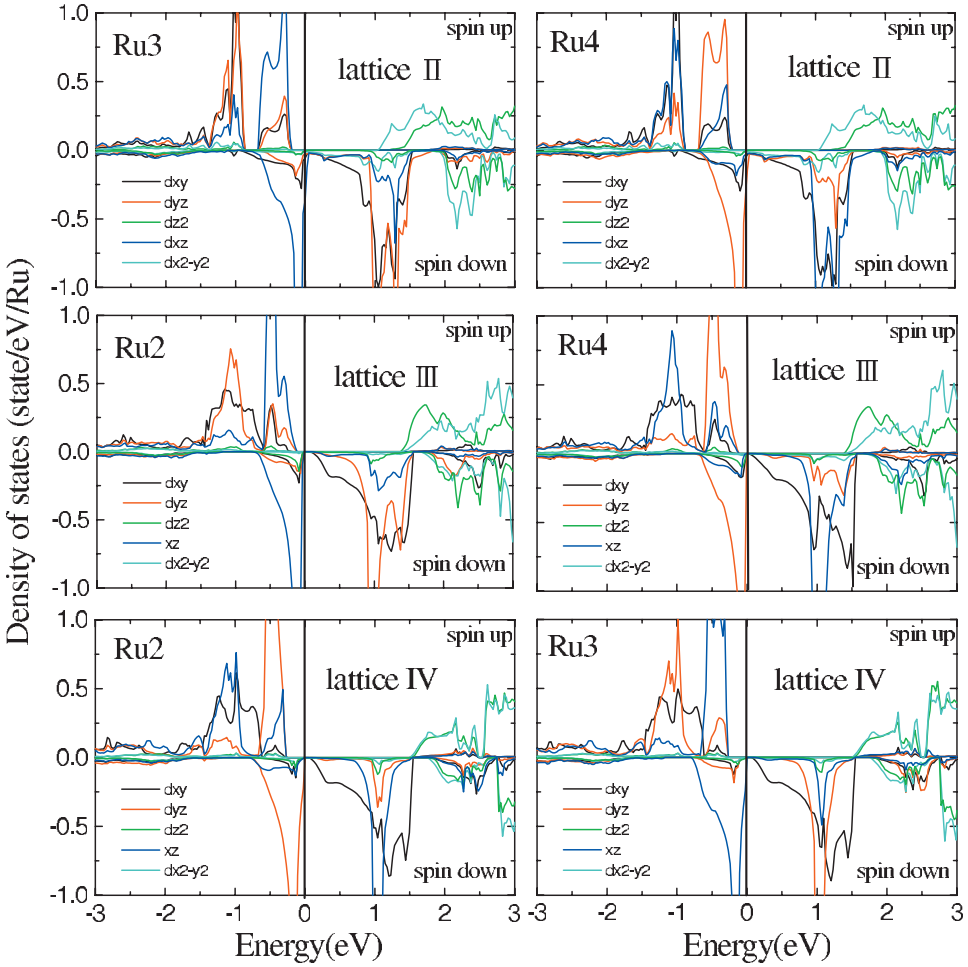

FIG. 9. (Color) Partial DOSs of Ru ions in $SrRu_{0.5}Ti_{0.5}O_3$ for lattice II (top panels), III (middle panels), and IV (bottom panels) from GGA+U calculations.

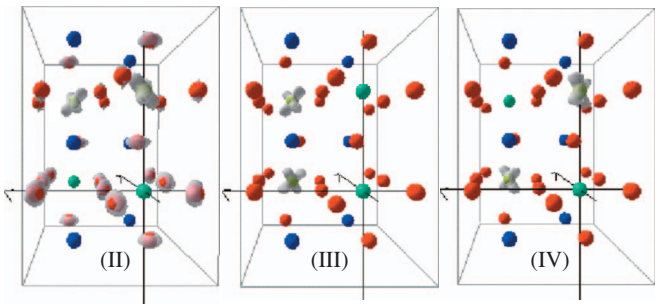

FIG. 10. (Color) Orbital-ordering patterns of $SrRu_{0.5}Ti_{0.5}O_3$ in lattices II (left), III (middle), and IV (right). The blue, green, light blue, and red balls denote Sr, Ru, Ti, and O ions, respectively. The gray color illustrates the charge contour of the occupied spin-down Ru t_{2g} band.

smaller than those of the $4d$ Ru^{4+} ions, leading to a relatively contracted TiO_6 octahedron. Consequently a Ti dopant at a Ru1 site results in an expanded coplanar $Ru2O_6$ octahedron especially in the lattice a-b plane, and therefore lowers the d_{xy} band energy of Ru2. Similarly, the smaller TiO_6 associated with the planar electron cloud distributions in $Ru2O_6$ also enlarges the second-layer $Ru3O_6$ and $Ru4O_6$ octahedra along the lattice c direction, and thus gives rise to lower d_{xz} and d_{yz} band energies, respectively, as shown in the orbital ordering contour of the occupied spin-down t_{2g} band in Fig. 8(b).

The partial DOSs of Ru ions in $SrRu_{0.5}Ti_{0.5}O_3$ for lattices II (top panels), III (middle panels), and IV (bottom panels) from GGA+U calculations are depicted in Fig. 9. In all the x=0.5 cases, the three t_{2g} bands in the majority spin channel of the two Ru ions are all fully occupied with one band (d_{xz} or d_{yz}) higher than the other two bands, while in the minority spin channel, there is approximately one d_{xz} or d_{yz} band occupied. One can see the good correspondence between the occupied spin-down t_{2g} band and the higher spin-up t_{2g} band due to the stronger Coulomb repulsion in the same t_{2g} orbital with one extra spin-down electron. It can also be seen that the two Ru ions in the three lattices are occupied by different spin-down t_{2g} electrons, i.e., d_{xz} and d_{yz} electron clouds reside respectively at Ru3 and Ru4 sites in lattice II, at Ru2 and Ru4 sites in lattice III, and at Ru3 and Ru2 in lattice IV. For all cases, the spin-down d_{xy} bands are energetically unfavorable around 1 eV above E_f. Figure 9 clearly indicates the different orbital-ordered ground states of lattices II–IV as demonstrated in the charge contour of the occupied spin down t_{2g} bands of Fig. 10.

In comparison with the orbital ordering of the undoped $SrRuO_3$ (Fig. 4 of Ref. 20), the electron cloud distributions on Ru sites in the planar lattice II and diagonal lattice IV are to some extent similar to those of the undoped case with the d_{xy} components significantly suppressed (Fig. 10). The high d_{xy} orbital energy is a natural consequence of the smaller TiO_6 octahedra in both the apical (lattice c) directions of RuO_6 since the elongation of the RuO_6 octahedra in the apical direction would lower the d_{xz} and d_{yz} orbital energies. In contrast, in the chain-type lattice III, the Ru2 ion exhibits a d_{yz} rather than a d_{xz} electron in $SrRuO_3$, which is presumably due to a better isotropy of the electron clouds in the ab plane,

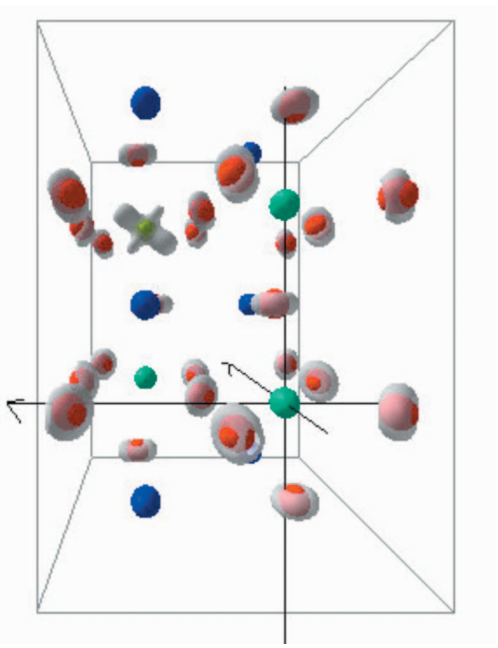

FIG. 11. (Color) Charge contour (gray) of the occupied spin-down Re t_{2g} band for $SrRu_{0.25}Ti_{0.75}O_3$ (lattice V). The blue, green, light blue, and red balls denote Sr, Ru, Ti, and O ions, respectively.

and therefore the more symmetric atomic positions and lattice structure of lattice III.

Figure 11 illustrates the charge contour of the occupied minority spin Ru t_{2g} bands of $SrRu_{0.25}Ti_{0.75}O_3$ from GGA+U calculations. It can be seen that with three Ti dopants in one unit cell, the only Ru site still exhibits a crosslike charge distribution with two major collinear lobes and the other two minor collinear lobes. Orbital character analysis shows that this asymmetric crosslike orbital has $4d$ t_{2g} features in the octahedral symmetry, which is a complicated linear superposition of the three t_{2g} orbitals. In this high-dosage case, the first and second nearest neighbors of the $Ru4O_6$ octahedron are all TiO_6 octahedra; therefore the $Ru4O_6$ octahedron can expand equally in all directions to provide a better accommodation for the electron clouds. Meanwhile, two of the adjacent coplanar oxygens (right-hand side) in $Ru4O_6$ move upward, making the higher octant narrower and the lower octant broader, whereas the other two coplanar oxygens (left-hand side) move in the opposite way, giving rise to the two major lobes within the larger octants and the minor lobes within the smaller octants as shown in Fig. 11.

Recent x-ray absorption spectroscopy measurement of the orbital population of the Ru ion in Ca_2RuO_4 reveals approximately 0.5 and 1.5 holes in the d_{xy} and $d_{yz/zx}$ orbitals, respectively.[28] Calculations using the LDA+U method also illustrate the ratio of hole populations $d_{xy}:d_{yz/zx}$ to be 0.5:1.5 for the orbital-ordered $SrRuO_3$.[20] In our case, the orbital behaviors are different with different doping conditions. For x =0.25, there is conceptually one spin-down electron occupying each d_{xy}, d_{zx}, and d_{yz} orbital of the Ru2, Ru3, and Ru4 ions, respectively (Fig. 8), leaving the $d_{yz/zx}$, $d_{xy/yz}$, and $d_{zx/xy}$ orbitals empty. As a result, the hole populations per Ru ion are estimated to be 2/3 and 4/3 for d_{xy} and $d_{yz/zx}$ orbitals, respectively. Similarly, for all three x=0.5 cases where either

the d_{yz} or d_{zx} orbital is occupied in the two Ru ions (Figs. 9 and 10), the predicted hole populations in the d_{xy} and $d_{yz/zx}$ orbitals are 2/2 and 2/2 per Ru ion, respectively. As for the $x=0.75$ case, the evaluated ratios are 2/3 and 4/3, respectively, for the evenly occupied d_{xy}, d_{yz}, and d_{zx} orbitals (Fig. 11). Future experiments such as x-ray absorption spectroscopy[28] would clarify the evolution of the hole populations and therefore the orbital behaviors upon varying the Ti concentrations.

IV. CONCLUSION

The electronic structures of $SrRu_{1-x}Ti_xO_3$ with x of 0.25, 0.50, and 0.75 have been systematically investigated using the GGA and GGA+U methods. The GGA calculations lead to a metal to half-metal transition at $x\approx0.5$, in disagreement with the experimental observation of a MIT upon variation of the dopant concentration. In contrast, an on-site Coulomb repulsion U of 3.5 eV gives rise to a MIT at $x\approx0.5$, close to the observed MIT at $x\approx0.3$, demonstrating that the MIT is driven primarily by the electron correlations. A larger U would further push the MIT toward a smaller Ti dosage, closer to the experimental result. The good agreement between the GGA+U results and the experimental observations reveals that the electron correlation plays an important role in $SrRu_{1-x}Ti_xO_3$. On the other hand, we have also investigated in detail the effects of Ti dopants on the orbital ordering. It is found that the Ti impurities with negligible valence electrons and smaller atomic size significantly affect the Jahn-Teller distortions and therefore achieve strong evolution in the orbital-ordering pattern upon Ti dosage.

ACKNOWLEDGMENTS

This work was supported by the National Science Council of Taiwan. We also thank NCHC, CINCNTU, and NCTS for technical support.

*jeng@phys.sinica.edu.tw

[1] Y. Maeno, H. Hashimoto, K. Yoshida, S. Nishizaki, T. Fujita, J. G. Bednorz, and F. Lichtenberg, Nature (London) **372**, 532 (1994).
[2] C. S. Alexander, G. Cao, V. Dobrosavljevic, S. McCall, J. E. Crow, E. Lochner, and R. P. Guertin, Phys. Rev. B **60**, R8422 (1999).
[3] J. S. Ahn, J. Bak, H. S. Choi, T. W. Noh, J. E. Han, Y. Bang, J. H. Cho, and Q. X. Jia, Phys. Rev. Lett. **82**, 5321 (1999).
[4] P. Kostic, Y. Okada, N. C. Collins, Z. Schlesinger, J. W. Reiner, L. Klein, A. Kapitulnik, T. H. Geballe, and M. R. Beasley, Phys. Rev. Lett. **81**, 2498 (1998).
[5] G. Cao, S. McCall, M. Shepard, J. E. Crow, and R. P. Guertin, Phys. Rev. B **56**, 321 (1997).
[6] K. Fujioka, J. Okamoto, T. Mizokawa, A. Fujimori, I. Hase, M. Abbate, H. J. Lin, C. T. Chen, Y. Takeda, and M. Takano, Phys. Rev. B **56**, 6380 (1997).
[7] J. Okamoto, T. Mizokawa, A. Fujimori, I. Hase, M. Nohara, H. Takagi, Y. Takeda, and M. Takano, Phys. Rev. B **60**, 2281 (1999).
[8] J. Park, S. J. Oh, J. H. Park, D. M. Kim, and C. B. Eom, Phys. Rev. B **69**, 085108 (2004).
[9] J. Kim, J. Chung, and S. J. Oh, Phys. Rev. B **71**, 121406(R) (2005).
[10] M. Takizawa, D. Toyota, H. Wadati, A. Chikamatsu, H. Kumigashira, A. Fujimori, M. Oshima, Z. Fang, M. Lippmaa, M. Kawasaki, and H. Koinuma, Phys. Rev. B **72**, 060404(R) (2005).
[11] A. Georges, G. Kotliar, W. Krauth, and M. J. Rozenberg, Rev. Mod. Phys. **68**, 13 (1996).
[12] P. W. Anderson, Phys. Rev. **109**, 1492 (1958); E. N. Economou and M. H. Cohen, Phys. Rev. Lett. **25**, 1445 (1970).
[13] S. L. Cuffini, V. A. Macagno, R. E. Carbonio, A. Melo, E. Trollund, and J. L. Gautier, J. Solid State Chem. **105**, 161 (1993).
[14] R. F. Bianchi, J. A. G. Carrió, S. L. Cuffini, Y. P. Mascarenhas, and R. M. Faria, Phys. Rev. B **62**, 10785 (2000).
[15] K. W. Kim, J. S. Lee, T. W. Noh, S. R. Lee, and K. Char, Phys. Rev. B **71**, 125104 (2005).
[16] J. Kim, J. Y. Kim, B. G. Park, and S. J. Oh, Phys. Rev. B **73**, 235109 (2006).
[17] S. B. Wilkins, P. D. Spencer, P. D. Hatton, S. P. Collins, M. D. Roper, D. Prabhakaran, and A. T. Boothroyd, Phys. Rev. Lett. **91**, 167205 (2003).
[18] D. J. Huang, H.-J. Lin, J. Okamoto, K. S. Chao, H.-T. Jeng, G. Y. Guo, C.-H. Hsu, C.-M. Huang, D. C. Ling, W. B. Wu, C. S. Yang, and C. T. Chen, Phys. Rev. Lett. **96**, 096401 (2006).
[19] Horng-Tay Jeng, G. Y. Guo, and D. J. Huang, Phys. Rev. Lett. **93**, 156403 (2004).
[20] Horng-Tay Jeng, Shi-Hsin Lin, and Chen-Shiung Hsue, Phys. Rev. Lett. **97**, 067002 (2006).
[21] P. E. Blöchl, Phys. Rev. B **50**, 17953 (1994); G. Kresse and D. Joubert, *ibid.* **59**, 1758 (1999).
[22] G. Kresse and J. Hafner, Phys. Rev. B **48**, 13115 (1993); G. Kresse and J. Furthmüller, Comput. Mater. Sci. **6**, 15 (1996); Phys. Rev. B **54**, 11169 (1996).
[23] J. P. Perdew and Y. Wang, Phys. Rev. B **45**, 13244 (1992).
[24] A. I. Liechtenstein, V. I. Anisimov, and J. Zaanen, Phys. Rev. B **52**, R5467 (1995).
[25] M. Shikano, T. K. Huang, Y. Inaguma, M. Itoh, and T. Nakamura, Solid State Commun. **90**, 115 (1994).
[26] I. V. Solovyev, P. H. Dederichs, and V. I. Anisimov, Phys. Rev. B **50**, 16861 (1994).
[27] M. Abbate, J. A. Guevara, S. L. Cuffini, Y. P. Macarenhas, and E. Morikawa, Eur. Phys. J. B **25**, 203 (2002).
[28] T. Mizokawa, L. H. Tjeng, G. A. Sawatzky, G. Ghiringhelli, O. Tjernberg, N. B. Brookes, H. Fukazawa, S. Nakatsuji, and Y. Maeno, Phys. Rev. Lett. **87**, 077202 (2001).